

Detection of the lithium depletion boundary in the young open cluster IC 4665 [★]

S. Manzi¹, S. Randich¹, W.J. de Wit^{2,3}, and F. Palla¹

¹ INAF-Osservatorio Astrofisico di Arcetri, Largo E. Fermi 5, I-50125 Firenze, Italy

² Laboratoire d'Astrophysique, Observatoire de Grenoble, BP 53, F-38041 Grenoble, Cédex 9, France

³ School of Physics & Astronomy, University of Leeds, Woodhouse Lane, Leeds LS2 9JT, UK

Received Date: Accepted Date

Abstract

Context. The so-called lithium depletion boundary (LDB) provides a secure and independent tool for deriving the ages of young open clusters.

Aims. In this context, our goal is to determine membership for a sample of 147 photometrically selected candidates of the young open cluster IC 4665 and to use confirmed members to establish an age based on the LDB.

Methods. Employing the FLAMES multi-object spectrograph on VLT/UT2, we have obtained intermediate-resolution spectra of the cluster candidates. The spectra were used to measure radial velocities and to infer the presence of the Li I 670.8 nm doublet and H α emission.

Results. We have identified 39 bona fide cluster members based on radial velocity, H α emission, and Li absorption. The mean radial velocity of IC 4665 is found to be $V_{\text{rad}} = -15.95 \pm 1.13$ km/s. Confirmed cluster members display a sharp transition in magnitude between stars with and without lithium, both in the I_m vs. $I_m - z$ and in the K_s vs. $I_C - K_s$ diagrams. From this boundary, we deduce a cluster age of $27.7_{-3.5}^{+4.2} \pm 1.1 \pm 2$ Myr.

Conclusions. IC 4665 is the fifth cluster for which an LDB age has been determined, and it is the youngest cluster among these five. Thus, the LDB is established from relatively bright stars still in the contracting pre-main sequence phase. The mass of the boundary is $M_* = 0.24 \pm 0.04 M_{\odot}$. The LDB age agrees well with the ages derived from isochrone fitting of both low and high mass, turn-off stars, a result similar to what is found in the slightly older NGC 2547.

Key words. open clusters and associations: individual: IC 4665 – stars: low-mass – stars: pre-main-sequence – stars: abundances

1. Introduction

Pre-main sequence (PMS) clusters with an age of 5-50 Myr represent an ideal tool for investigating several aspects related to star formation and the early phases of (sub-)stellar evolution. These clusters provide the youngest samples of PMS stars outside a star forming environment. Indeed, unlike star forming regions, PMS clusters show the complete and final product of the formation process, immediately after the active phase of star birth. Moreover, the low-mass members (both stars and brown dwarfs) are still bright and readily detectable, and not affected by severe extinction since most of the circumstellar and interstellar material has been accreted and dispersed. Finally, the age interval of PMS clusters is critical with respect to the early evolution of protoplanetary disks, stellar rotation, and activity. Despite these benefits, at present only three systems are confirmed PMS clusters: NGC 2547 (~35 Myr; Jeffries & Oliveira 2005), NGC 2169 (~10 Myr; Jeffries et al. 2007), IC 2391 (~50 Myr; Barrado y Navascués et al. 2004); a few other candidates exist. The identification of additional PMS

cluster candidates and confirmation of their nature through a secure age determination would therefore represent a significant improvement from the phenomenological and statistical point of view (see discussion in Jeffries et al. 2007).

Ages of stellar clusters can be obtained from the location of the main sequence turn-off (t_{nuc1}) or from the isochronal distribution of the PMS population in the HR diagram. These classical methods are widely used, but suffer from large uncertainties of up to a factor of two in age (e.g., Mermilliod 2000; Jeffries & Oliveira 2005). On the contrary, the method based on the lithium depletion boundary (LDB) has proven to be robust and less model dependent since it relies on well known physics (Bildsten et al. 1997; Ushomirsky et al. 1998). During the PMS phase, stars undergo a gradual gravitational contraction that causes a progressive, mass-dependent rise of the central temperature. Li burning starts when the core reaches a temperature $\approx 3 \times 10^6$ K (depending on density); hence, in fully convective low-mass stars ($M \lesssim 0.5 M_{\odot}$) Li is depleted from the initial interstellar abundance on a time scale that is a sensitive function of mass. In a young stellar cluster three regimes of Li depletion are present: i) relatively massive stars (with radiative interiors) that suffer only a little amount of Li depletion; ii) stars in the so-called Li chasm (Basri 1997) that have

Send offprint requests to: S. Randich, email:randich@arcetri.astro.it

[★] Based on observations collected at ESO-VLT, Paranal Observatory, Chile. Program number 073.D-0587(A).

fully depleted their initial Li supply; iii) low mass stars that have preserved the initial Li content. The transition between low-mass stars with and without Li is very sharp and the luminosity of the faintest star that has depleted 99 % of its initial Li identifies the boundary (LDB) and the age (t_{LDB}) of the cluster (e.g., Basri et al. 1996; Basri 1997; Stauffer 2000). The older the cluster is, the fainter the stars at the boundary are. So far, the LDB has been detected in four clusters: the Pleiades (Stauffer et al. 1998), α Persei (Stauffer et al. 1999), IC 2391 (Barrado y Navascués et al. 2004), and NGC 2547 (Jeffries & Oliveira 2005). Remarkably, the LDB ages determined for the Pleiades, α Per, and IC 2391 exceed the nuclear ages by a factor ~ 1.5 ; these particular nuclear ages were derived from fitting the cluster turn-off (TO) with evolutionary models without overshooting. On the other hand, the two dating methods yield similar ages for the younger cluster NGC 2547, although the cluster’s nuclear age is still rather uncertain.

In this paper, we report on the determination of the LDB in the open cluster IC 4665 whose properties have been extensively discussed by de Wit et al. (2006). IC 4665 is an interesting candidate PMS cluster, located relatively far from the Galactic plane at $b \sim +17^\circ$. Its nuclear age is about $t_{\text{nucl}} = 36$ Myr (Mermilliod 1981), but other properties might suggest an age as high as 100 Myr (Prosser 1993). The Hipparcos distance is 385 ± 40 pc (Hoogerwerf et al. 2001), while a lower value of 320 pc has been derived by Crawford & Barnes (1972). IC 4665 was targeted for a wide and deep survey in I_m (Mould) and z filters at the Canada-France-Hawaii telescope (CFHT). This deep photometric survey led to the detection of 786 new low-mass stellar and brown dwarf candidate members ($14.8 < I_m < 22$), down to about $30M_{\text{Jup}}$ (de Wit et al. 2006). Given the nuclear age of IC 4665, the new low-mass candidate members provide a sample suitable for the detection of the LDB and for the derivation of an accurate and independent age estimate. The importance of such determination was already stressed by Martín & Montes (1997) who were the first to obtain Li abundances in a small sample of cluster stars (mainly of G and early-K spectral-type). Although a spread in Li was found, the observations did not reach the low luminosity population of IC 4665 where the LDB is expected to occur.

Our paper is structured as follows: Section 2 describes the sample selection, observations, and data analysis. The results on membership and the lithium boundary are given in Section 3. The age of IC 4665 and the comparison with other young PMS clusters is discussed in Section 4. The conclusions close the paper.

2. Sample selection, observations and data analysis

Target stars were selected from different sources: Prosser (1993), Giampapa et al. (1998), de Wit et al. (2006), and a literature search on SIMBAD. The sample includes 96 stars from Prosser (1993 –of these, 88 were covered by the CFHT survey, but not included in the catalog of de Wit et al.), one star from Giampapa et al. (1998), 15 stars from de Wit et al. (2006), 24 stars included both in Prosser and de Wit et al. catalogs, and eight new candidate members. The latter

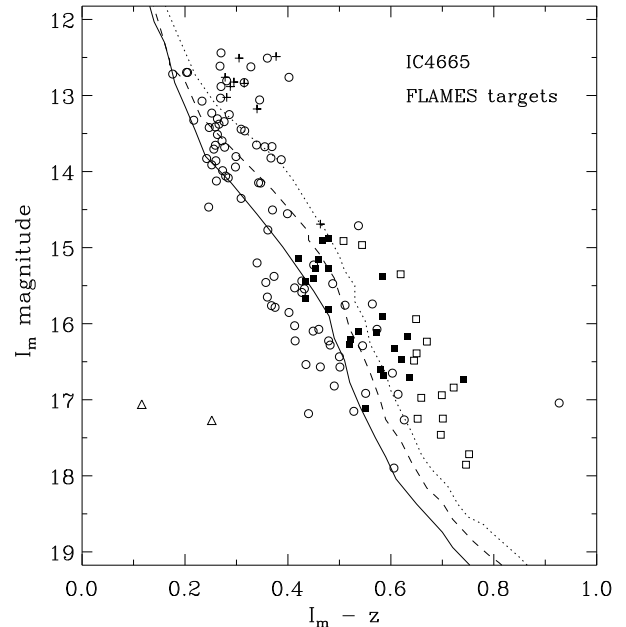


Figure 1. I_m vs. $I_m - z$ color-magnitude diagram of all the 137 candidate members observed with Giraffe and with available photometry from the CFHT survey. Target stars have been retrieved from **i.** Prosser (1993) and Giampapa et al. (1998): open circles, 89 stars; **ii.** de Wit et al. (2006), open squares and crosses – 15 and eight stars, respectively; **iii.** Luyten (1961): triangles, two stars. Filled squares instead represent candidates common to Prosser and de Wit et al. (24 stars). Crosses are the eight objects brighter than the minimum magnitude selection limit in de Wit et al. and not reported in Prosser. Three isochrones for 30, 50, and 100 Myr are shown from the Nextgen model of Baraffe et al. (1998) with a mixing length parameter $\alpha = 1$ and for a distance of 370 pc (see Sect. 3.2).

had been selected by de Wit et al., but were not included in their final analysis since they are brighter than $I_m = 14.8$ mag, the cutoff limit used in that paper. Finally, we also observed two stars from Luyten (1961) and one IRAS source (IRAS 17447+054), since they happen to lie in the FLAMES target fields. The present sample hence consists of a total of 147 stars. Of these, a subsample of 137 candidate cluster members have I_m and z photometry available from the CFHT survey. Fig. 1 shows their distribution in the color-magnitude diagram. Stars with I_m magnitudes between ~ 16 and 18 bracket the expected apparent brightness of the LDB boundary at the distance of IC 4665 corresponding to a relatively young (~ 20 Myr) and old (~ 50 Myr) age. The 147 target stars are listed in Table 1 that gives a running number (Col. 1); coordinates (Cols. 2-3); data source (Col. 4: 1- only in Prosser or Giampapa et al.; 2- from Prosser and de Wit et al.; 3- only in de Wit et al.; 4- not in Prosser nor in de Wit et al. because brighter than the I_m limit of that paper; 9- from IRAS or Luyten); name (Col. 5); I_m and z magnitudes (Col. 6-7); radial velocity and associated error (Col. 8-9; a “-” means that we were not able to measure the velocity); presence (Y) or lack (N) of the Li line (Col.

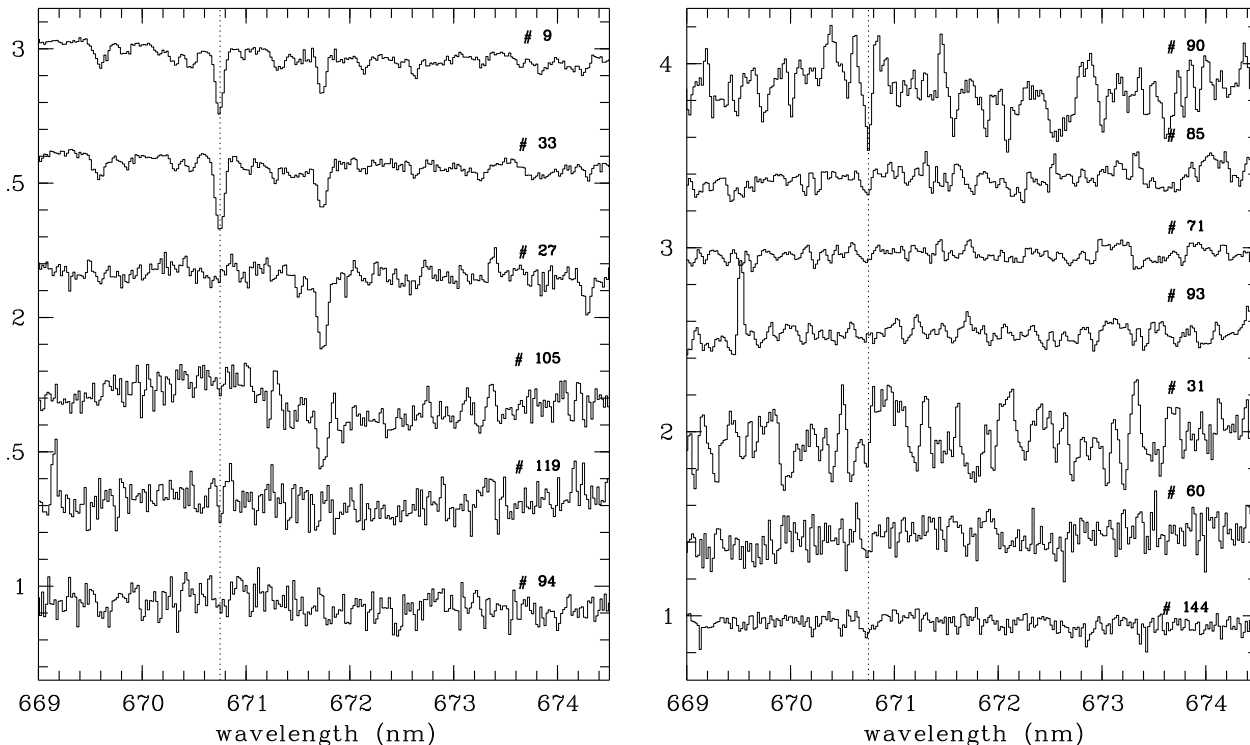


Figure 2. Spectra of 13 stars ordered by increasing magnitude representative of the Li range: above the chasm (#9 and #33), in the chasm (#27 and #105), and close and below the the LDB (#119, #94, #90, #85, #71, #93, #31, #60, #144). The vertical dashed line at 607.8 nm marks the expected Li line position. Note that the TiO bands at wavelengths redder than ~ 672 nm are not visible in the spectra with very low S/N due to poor sky subtraction.

10: “?” means that the S/N did not allow to confirm or reject the presence of Li); presence of the $H\alpha$ line in absorption or emission (Col. 11); and membership flag (Col. 12 –see Sect. 3.1). The I_m and z magnitudes listed in the table are from the CFHT measurements. Note that for a large fraction of these objects VI photometry in the Kron system is also available from Prosser (1993) and that near-infrared photometry for all the stars was retrieved from the Two Micron All Sky Survey (2MASS) catalogue. In the following, we will use our running numbers given in Col. 1.

The observations were carried out in Service Mode during May, June, July, and September 2004 using the FLAMES instrument (Pasquini et al. 2002) on VLT/UT2. The spectra were obtained with the GIRAFFE spectrograph in conjunction with the MEDUSA fibre system and a 600 lines/mm grating (L6). The resolving power is $R \sim 8000$, and the exposure time chosen to reach a S/N ratio ~ 20 for the faintest targets. The spectra cover the wavelength range between 643.8 nm and 718.4 nm, which includes the $H\alpha$ line, besides the Li I 607.8 nm resonance doublet. The stars were observed in two configurations, A and B, covering two different fields. The configurations were centered at RA(2000)=17h 46m 46.27s and DEC(2000)=+05d 38m 17.7s, and RA(2000)=17h 45m 26.91s and DEC(2000)=+05d 56m 53.7s, respectively. 94 and 53 stars were allocated in configurations A and B. We obtained six 45 min exposures for configuration A and four 45 min exposures for configuration B.

Data reduction was performed using Giraffe BLDRS¹, following the standard procedure and steps (Blecha & Simond 2004). The sky contribution was subtracted separately; namely, for each configuration, we considered 15 sky spectra, subdivided them in three groups of five spectra, and derived the median sky from each group. Then, we formed a “master” sky by taking the average of the three median sky spectra. Due to the fact that the sky on the CCD was rather inhomogeneous and to the presence of scattered light from the fibers allocated to very bright objects, for the faint stars an appropriate sky subtraction was impossible to perform. For this reason, while both the Li and $H\alpha$ lines when present are in most cases clearly visible in the spectrum, we prefer not to give any quantitative measurement of their equivalent widths.

Data handling and analysis has been carried out both with MIDAS and IRAF² software packages. In most cases multiple sky-subtracted spectra of the same target have been combined, after adjusting them for Doppler shift due to the motion of the earth after sky subtraction. For a few stars we excluded one or more exposures, due to bad quality. Final S/N ratios per resolution element are in the range $\sim 200 - 15$. In Fig. 2 we present some representative spectra spanning the magnitude range cor-

¹ version 1.12 – <http://girbldrs.sourceforge.net/>

² IRAF is distributed by the National Optical Astronomical Observatories, which are operated by the Association of Universities for Research in Astronomy, under contract with the National Science Foundation.

responding to the three regimes mentioned in Sect. 1: solar-type stars with a strong Li line; stars lacking Li that fall in the Li chasm; stars below the LDB, showing again the Li feature.

Radial velocities (V_{rad}) have been measured from the average shift of the spectral lines in the co-added spectra. For some critical spectra (e.g. low S/N, suspected binary) we have determined V_{rad} from the individual exposures. Measurements of V_{rad} were carried out using IRAF and the *RVIDLINES* procedure. We typically used 10-20 lines per star, depending on S/N. For the faintest stars, V_{rad} was determined using a couple of lines only. Resulting heliocentric radial velocities have errors between 0.5 and 6 km/sec and are listed in Cols. 8 and 9 of Table 1.

3. Results

3.1. Membership

In order to confirm or reject membership of the cluster candidates, we applied the usual radial velocity criterion, together with the requirement on the presence of Li (for bright stars) and/or $H\alpha$. We have first estimated the cluster average V_{rad} and its standard deviation from the observed V_{rad} distribution of the sample. In Fig. 3 we show the distribution of measured radial velocities (stars with variable V_{rad} are obviously not included in the figure): there is a clear peak at $V_{\text{rad}} \approx -15$ km/s which indicates the presence of the cluster. The average velocity was derived by fitting the observed distributions with two gaussian functions, one for the cluster and one for field stars; the best fit was then determined using a maximum likelihood algorithm. For IC 4665 we find $V_{\text{rad}}(\text{IC 4665}) = -15.95$ km/s and $\sigma(\text{IC 4665}) = 1.13$ km/s, while for the field we obtain $V_{\text{rad}}(\text{field}) = -15.87$ km/s and $\sigma(\text{field}) = 48.63$ km/s. Interestingly, the field and cluster velocities are very similar, although, as expected, the distribution of the field stars is much broader. The cluster average velocity is compatible with previous estimates, notably that from the high-mass members *viz.* $V_{\text{rad}} = -15.5$ km/s and $\sigma = 2.9$ km/s (Crampton et al. 1976). On the other hand, Prosser & Giampapa (1994) found the slightly higher value of $V_{\text{rad}} = -13$ km/s. We have considered as cluster members those stars with V_{rad} within $\pm 3\sigma$ from the average value. In addition, we have also included three stars (#55, #87, and #138) with V_{rad} slightly outside this limit, but with large errors on V_{rad} and with other indicators consistent with membership (see below). With this criterion 42 radial velocity members were found, with an expected statistical contamination (i.e., non members with V_{rad} consistent with the cluster) of five stars, as estimated from the fitting procedure. Furthermore, 14 possible members with variable radial velocity and/or evidence for a double line system were considered as possible members. Thus, we have a total of 56 possible candidates.

The presence of $H\alpha$ emission and/or Li absorption provides additional membership criteria for the V_{rad} members and for stars without a radial velocity measurement. In Fig. 4 we show the same color-magnitude (CM) diagram of Fig. 1, but with the additional information on V_{rad} and $H\alpha$ of each individual star. The figure clearly shows that stars with $I_m \gtrsim 14$ must have $H\alpha$ emission in order to be members. Therefore, we considered as

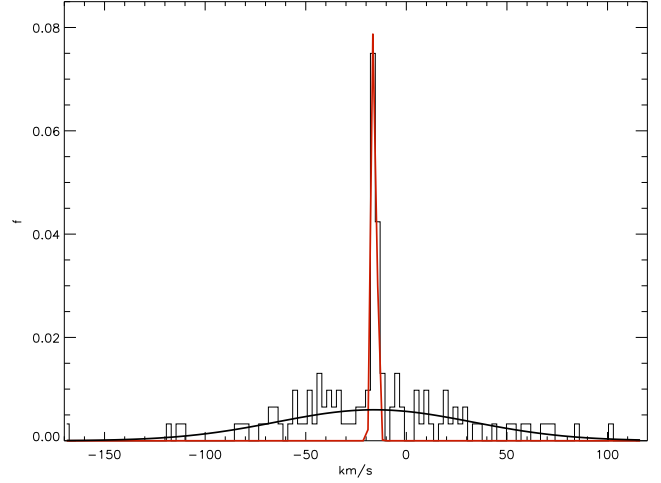


Figure 3. Radial velocity distribution of IC 4665 candidate

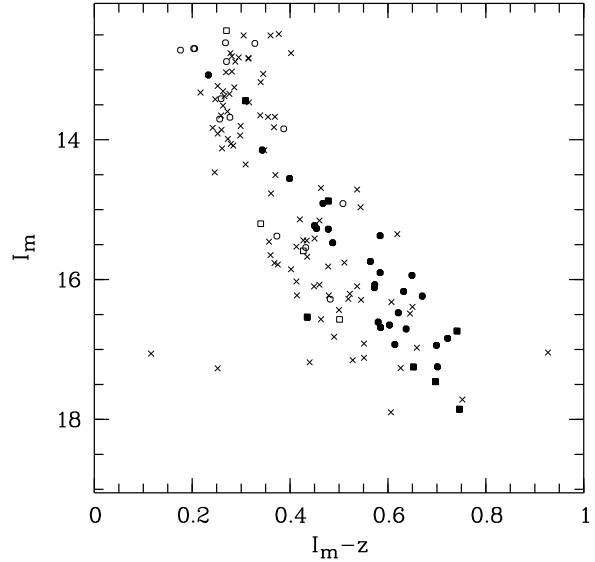


Figure 4. CM diagram of the observed targets with available I_z photometry including information on V_{rad} and presence of $H\alpha$ emission. Symbols are as follows: open circles - V_{rad} members without $H\alpha$ emission; filled circles - V_{rad} members with $H\alpha$ emission, including the three marginal V_{rad} members; open squares - V_{rad} variables without $H\alpha$ emission; filled squares - V_{rad} variables with $H\alpha$ emission or "abs/em"; crosses - all other stars.

non members all stars fainter than this magnitude limit without $H\alpha$ emission: we found 10 such stars (#2, #36, #41, #44, #48, #49, #67, #81, #126, #139), four of them with V_{rad} consistent with membership, and six with variable V_{rad} . We also discarded the star #129 which does not show the Li line, in spite of having a magnitude brighter than the Li chasm, as well as stars #5 and #141, with no available photometry, but lacking both Li and $H\alpha$. Interestingly, the number of stars with consistent V_{rad} , but not satisfying the $H\alpha$ /Li criteria (seven) is comparable to

Table 2. Stars confirmed as members. The values for I_c are converted from I_m , as explained in the text.

#	I_m (mag)	$I_m - z$ (mag)	$I_c - K_s$ (mag)	EW(Li) (mÅ)	#	I_m (mag)	$I_m - z$ (mag)	$I_c - K_s$ (mag)	EW(Li) (mÅ)	#	I_m (mag)	$I_m - z$ (mag)	$I_c - K_s$ (mag)	EW(Li) (mÅ)
20	12.440	0.270	1.639	30±4	72	14.876	0.478	2.449	—	100	16.475	0.621	2.709	—
6	12.614	0.268	1.771	52±5	88	14.910	0.467	2.287	—	69	—	—	—	—
9	12.623	0.328	1.343	235±5	95	15.228	0.450	2.482	—	119	16.608	0.580	2.506	Y?
26	12.696	0.203	1.243	255±7	147	15.269	0.454	2.302	—	94	16.650	0.603	2.710	Y?
33	12.697	0.205	1.291	274±7	105	15.278	0.477	2.369	—	90	16.685	0.585	2.665	Y
74	12.718	0.176	1.255	245±10	145	15.373	0.584	2.591	—	85	16.706	0.637	2.661	Y
62	13.074	0.233	1.567	236±8	55	15.474	0.487	2.412	—	71	16.736	0.741	2.965	Y
16	13.413	0.259	1.569	35±4	98	15.741	0.564	2.590	—	93	16.840	0.722	2.730	?
59	13.443	0.309	1.959	70±3	87	15.902	0.584	2.545	—	31	16.928	0.614	2.747	?
125	13.680	0.277	1.699	31±4	82	15.940	0.649	2.579	—	60	16.940	0.699	2.860	Y
83	13.705	0.256	1.748	—	28	16.074	0.573	2.484	—	144	17.248	0.701	2.896	Y
142	13.844	0.387	2.464	—	128	16.116	0.572	2.550	—					
27	14.147	0.343	1.959	—	121	16.169	0.632	2.720	—					
120	14.554	0.399	2.262	—	138	16.236	0.670	2.814	—					

that of the expected number of contaminants. Finally, we note the presence of four stars with uncertain membership status, because we could not retrieve enough/secure information from their spectra. One of them, star #11, is a SB2 system with $H\alpha$ emission and uncertain Li status; given its position in the CM diagram (below the sequence), it is likely a non member. A final membership flag is given in Col. 12 of Table 1. Specifically, we assigned a “Y” status to stars with secure membership and consistency between all indicators; we marked “Y?” stars with two indicators (out of three) consistent with membership and the three stars with V_{rad} slightly outside the permitted range, while we gave uncertain status (“?”) to the four stars with variable radial velocity, $H\alpha$ emission, and uncertain Li line. Finally, stars that turned out to be non members are marked with “N”. In summary, of the 147 candidates, 39 stars are members (Y or Y? status), 104 non members, and 4 with uncertain membership. The 39 confirmed members are listed in Table 2, where we also give the Li equivalent widths for the brighter objects and the presence of the Li line for the faintest ones.

Our analysis indicates that 27% of the sample stars are likely cluster members, in reasonable agreement with the estimate of de Wit et al. (2006). A detailed discussion of membership and contamination in different mass bins cannot be presented here, since not only our spectroscopic sample is incomplete as a whole, but stars in different mass bins are characterized by varying degrees of completeness. This discussion is deferred to a forthcoming paper (de Wit et al. in preparation) where the analysis of a much larger sample of very low-mass cluster stars and brown dwarfs will be presented, based on low resolution optical and near-IR spectra.

3.2. The absolute brightness of the Li boundary

In Fig. 5 we show the I_m vs. $I_m - z$ and K_s vs. $I_c - K_s$ color-magnitude diagrams of the 38 likely cluster members listed in Table 2 with available photometry.

A chasm and boundary are clearly present in both diagrams. We determine the observed LDB of IC 4665 from the bright-

est star with secure Li detection (“Y” status in Table 2) on the faint side of the chasm. In the I_m vs. $I_m - z$ diagram this corresponds to the star #90 with $I_m = 16.68$. Note that, whereas the Li line might be present in the spectra of stars #119 and #94 (classified as “Y?” in Table 2), the lower S/N of these two spectra makes the detection of Li less secure than in the case of star #90. Alternatively, the theoretical LDB could also be defined by the faintest star within the chasm. In such a case, the LDB of IC 4665 would correspond to the star #100 with $I_m = 16.47$ mag

For most of faint members in this paper, standard V_{Ic} photometry is not available. In order to convert Mould to Cousin I magnitudes, we used new photometry of IC 4665 that will be presented in James et al. (2008). More specifically, James et al. have performed a shallow survey of IC 4665 in BVI_{Ic} , allowing us to derive relationships both between $I_m - z$ and $V - I_c$ colors and between I_c and I_m magnitudes. The relation between $I_m - z$ and $V - I_c$ was obtained for objects present in both James et al. and de Wit et al. (2006) with $0.0 < I_m - z < 0.35$ or, correspondingly, $0.7 < V - I_c < 2.1$. We found $V - I_c = 0.65444 + 3 \times (I_m - z) + 3 \times (I_m - z)^2$. This was then extrapolated up to $I_m - z = 0.75$. Using the 1σ errors on the fit and extrapolating the 1σ upper and lower limit of the fit, delivers a range in values for $V - I_c$ of 0.3 mag. As to magnitude conversion, we directly compared I_m and I_c magnitudes of stars in common in the two surveys and found median values $I_c - I_m = 0.03$ and 0.06 for $I_m - z$ lower and greater than 0.2 mag, respectively. The typical scatter is 0.05 mag.

As a check, **1)** we estimated the expected $I_c - I_m$ difference for stars of different temperatures based on the filter transmission curves and found that it increases from ~ 0.03 mag at 6000 K to ~ 0.06 mag at 3500 K; **2)** we derived $V - I_c$ colors from $V - I_K$ colors published by Prosser (1993), employing the transformation of Bessel (1979); from these $V - I_c$ colors and V magnitudes given in Prosser, we also estimated I_c magnitudes. We found a good agreement between magnitudes and colors estimated in this way and those obtained extrapolating from

James photometry: namely, $\Delta(V-I_C)_{\text{mean}} = 0.02 \pm 0.1$ mag and $\Delta I_{C\text{mean}} = 0.1 \pm 0.28$ mag.

As mentioned in Sect. 1, the distance to IC 4665 is not accurately known with values ranging from 320 pc (Crawford & Barnes 1972) to $385+40=425$ pc (Hoogerwerf et al. 2001). Without convincing evidence for a short or a long distance, we adopt a compromise between the two extremes, i.e. a distance of 370 ± 50 pc. We have also estimated our own distance to IC 4665 by comparing the photometry ($V, B-V$) of high mass stars in IC 4665 to the Pleiades and determining a vertical offset. By assuming a distance to the Pleiades of 133 pc and $E(B-V)=0.03$, the best matching of the two sequences is obtained with a distance to IC 4665 equal to 366 pc, very close to our adopted average.

Taking $A(I_C)=0.333$ (from $E(B-V)=0.18$ –Hogg & Kron 1955- and the extinction law of Dean et al. 1978), we obtain for stars #100 and #90 $M_{I_C} = 8.37$ and 8.57 , respectively. Considering the average of the two values, we find that the LDB occurs at $M_{I_C} = 8.47^{+0.32}_{-0.28} \pm 0.10$ mag, where the first contribution to the error is due to uncertainty in distance and the second one reflects the uncertainty in the LDB determination. Clearly the error is dominated by the distance uncertainty.

Similarly, the brightest/faintest stars with/without Li in the K_s vs. I_C-K_s diagram are #90 ($K_s=14.08$) and #100 ($K_s=13.826$). Assuming $A_K = 0.06$ mag, this yields an LDB at $K_s=6.05^{+0.32}_{-0.28} \pm 0.13$.

3.3. The LDB age of IC 4665

The age of IC 4665 can now be determined using model calculations. Fig. 6 displays the time variation of the absolute I_C and K_s magnitudes of a star which has depleted 99 % of the initial Li abundance, according to the models of Chabrier & Baraffe (1997). The LDB age that we derive from the two diagrams for IC 4665 is very similar, namely $t_{\text{LDB}}(M(I_C)) = 28.4^{+4.2}_{-3.4}$ Myr and $t_{\text{LDB}}(M(K_s)) = 28.0^{+4.6}_{-3.8}$ Myr. Also shown in the figure are the LDBs for NGC 2547 and IC 2391. In Table 3 we summarize LDB magnitudes, ages, and masses for the three PMS clusters, and using different magnitudes. Ages and masses were determined using the models of Chabrier & Baraffe (1997); LDB magnitudes for IC 2391 and NGC 2547 were taken from Jeffries & Oliveira (2005). $M_{\text{bol}}(\text{LDB})$ for IC 4665 was computed starting from I_C and K_s absolute magnitudes using the bolometric corrections (BCs) of Leggett et al. (1996) as a function of $V-I$ and I_C-K_s colors. Those corrections were used by Jeffries & Oliveira (2005) and we assumed them for consistency; we found $M_{\text{bol}}(I_C) = 8.65$ and $M_{\text{bol}}(K_s) = 8.84$. In the previous section and in Table 3 we considered only the uncertainty due to distance and LDB determination. However other sources of error are present: *i.* Uncertainty in the I_m to I_C conversion (~ 0.05 mag), that also reflects into I_C-K_s colors and thus slightly affects BCs for K_s magnitudes (~ 0.01 mag); *ii.* uncertainty in the $I_m - z$ to $V-I_C$ conversion (~ 0.3) mag, that affects BCs for I_C magnitudes (by ~ 0.1 mag); *iii.* uncertainty in reddening, that should not be larger than 0.05 mag; *iv.* finally, the choice of the bolometric correction vs. color calibration. By using the calibrations of Bessel (1991) we would have obtained

~ 0.07 brighter M_{bol} values. Each of these errors is at most of the same order of the uncertainty in the LDB determination and results in an error of about 1 Myr in the LDB age. Remarkably, LDB ages listed in Table 3 are all within 2.4 Myr. In particular, the LDB age from I_C magnitude is very similar to that from K_s magnitude, that is not affected by the error due to magnitude conversion. The average of the four values listed in Table 3 is 27.7 ± 1.1 Myr. On top of this, one has to consider the error due to use of different evolutionary models, which is of the order of 2 Myr, as shown by Jeffries & Oliveira (2005). Summarizing, our LDB age for IC 4665 is $27.7^{+4.2}_{-3.5} \pm 1.1 \pm 2$ Myr, where for the error due to distance and LDB determination we took the average of the errors given in Table 3.

With an LDB age of 27.7 Myr, IC 4665 is the youngest of the known PMS clusters. As to the LDB mass, from Table 3 we see that for IC 4465 the Chabrier & Baraffe (1997) models yield a value of $M(\text{LDB}) = 0.24 M_{\odot}$, independent of the choice of the absolute magnitude. As expected, this mass is above that of NGC 2547 ($M(\text{LDB}) = 0.17 M_{\odot}$) and IC 2391 ($M(\text{LDB}) = 0.12 M_{\odot}$).

4. Discussion

4.1. The age of IC 4665

As mentioned in Sect. 1, prior to our estimate, Mermilliod (1981) was the first to determine a nuclear age for IC 4665 and included it in the age group of 36 Myr, along with IC 2391. Later studies have found that the cluster could be almost as old as the Pleiades (Prosser 1993; Prosser & Giampapa 1994), although Prosser (1993) noted that the sequence of cluster candidates in the I_K vs. I_C-K_s diagram was suggestive of a rather young age. Our analysis confirms the young age, making IC 4665 the youngest cluster for which the LDB has been detected, and, equally important, allows us to firmly establish its PMS status. In addition, the LDB age matches the nuclear age. This is similar to the case of NGC 2547 (Jeffries & Oliveira 2005), but at variance with IC 2391, α Per, and the Pleiades where the age estimates differ by a factor ~ 1.5 .

Although there is no definite explanation for the discrepancy between the TO and LDB ages, the difference is usually interpreted as evidence for the occurrence of some convective core overshooting in high-mass stars that could lengthen the duration of the main sequence life time. The question then arises why a large difference between TO and LDB ages is instead not found for the two youngest clusters NGC 2547 and IC 4665. One possibility is indeed that the amount of overshooting in models of massive stars is a step function of TO mass, with more overshooting needed for lower TO masses of the older clusters. Still, it is puzzling that IC 2391 and IC 4665 were originally included in the same age group by Mermilliod (1981), based on the CM and color-color diagrams for high mass stars. We suggest that a careful re-analysis and comparison of the two cluster upper main sequence photometry and CM diagrams should be performed, taking into account the possible effects of binaries and rotation. This, along with use of updated stellar evolution models including overshooting, might provide insights on this issue.

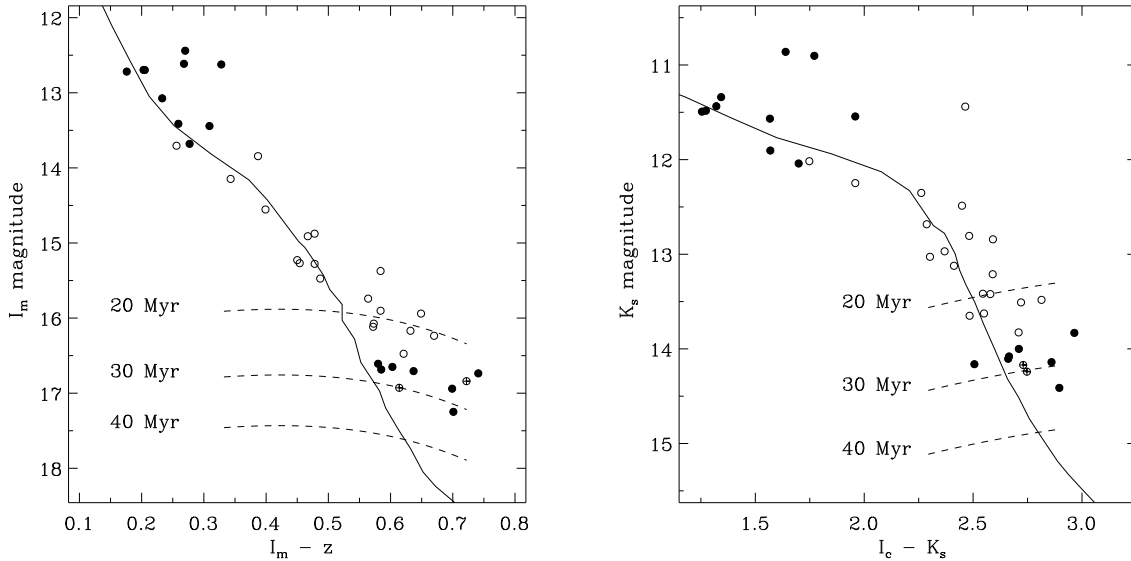


Figure 5. I_m vs. $I_m - z$ (left panel) and K_s vs. $I_c - K_s$ (right panel) diagrams of the 38 likely cluster members with available photometry listed in Table 2. Filled and open symbols indicate stars with detected/undetected Li line, respectively. The two crossed circles denote stars with uncertain Li detection. The theoretical position of the boundary from Chabrier & Baraffe (1997) models for ages of 20, 30, and 40 Myr is also shown (see text), along with the 30 Myr isochrone. Note that, by definition, the LDB is actually just a point on the isochrone. What we show here, following Jeffries & Oliveira (2005), are constant luminosity curves, with the luminosity corresponding to the LDB luminosity at a given age. These curves are not flat since, for a given M_{bol} , the bolometric correction changes with color (T_{eff}). To construct the curves, we estimated bolometric corrections for I_m and K_s as function of color from Baraffe et al. (1998) models.

Table 3. Properties of the LDB in IC 4665, NGC 2547, and IC 2391. The upper part lists the absolute magnitudes of the LDB. The bottom part gives the age and mass of the LDB derived from the three values of the absolute magnitudes listed in the upper part, using the Chabrier & Baraffe (1997) models with $\alpha = 1$. Errors are the quadratic sum of the uncertainty in distance and the uncertainty in the exact magnitude of the LDB.

	IC 4665	NGC 2547	IC 2391
M_{I_c}	$8.47^{+0.33}_{-0.30}$	9.33 ± 0.18	10.27 ± 0.14
M_{K_s}	$6.05^{+0.34}_{-0.31}$	6.74 ± 0.16	7.54 ± 0.14
$M_{bol}(I_c) = M_{bol1}$	$8.65^{+0.33}_{-0.30}$	9.58 ± 0.16	10.34 ± 0.14
$M_{bol}(K_s) = M_{bol2}$	$8.84^{+0.34}_{-0.31}$		
LDB(M_{I_c}): t (Myr); M (M_{\odot})	$28.4^{+4.2}_{-3.4}$; 0.24 ± 0.04	35.4 ± 3.3 ; 0.17 ± 0.02	49.1 ± 4.9 ; 0.12 ± 0.01
LDB(M_{K_s}): t (Myr); M (M_{\odot})	$28.0^{+4.6}_{-3.8}$; 0.24 ± 0.04	34.4 ± 2.7 ; 0.17 ± 0.02	50.4 ± 3.8 ; 0.12 ± 0.01
LDB(M_{bol1}): t (Myr); M (M_{\odot})	$26.1^{+4.1}_{-3.4}$; 0.24 ± 0.04	35.0 ± 2.2 ; 0.17 ± 0.02	48.8 ± 3.5 ; 0.12 ± 0.01
LDB(M_{bol2}): t (Myr); M (M_{\odot})	$28.3^{+4.0}_{-3.5}$; 0.24 ± 0.04		

4.2. Isochronal ages and comparison with other clusters

In Fig. 7 we compare the distribution of confirmed members of IC 4665, IC 2391, and NGC 2547 in the absolute K_s magnitude vs. $I_c - K_s$ diagram. The 20, 30, and 50 Myr isochrones and the predicted location of the LDB for different ages from Baraffe et al. (2002) are also shown, along with the ZAMS (solid line).

Comparison of isochrones and datapoints up to $I_c - K_s \sim 2.5$ suggests an age between 20 and 30 Myr (25 ± 5 Myr) for IC 4665 and NGC 2547, in excellent agreement with the LDB age of the former and slightly younger for the latter. At colors $I_c - K_s \gtrsim 2.5$ a larger scatter is present in both clusters, as well as a discrepancy between the data and the models. This dis-

crepancy has already been noted by Jeffries & Oliveira (2005) for NGC 2547, who found that the K_s vs. $I_c - K_s$ diagram gives an isochronal age smaller than optical diagrams. As a possible explanation, these authors note that model atmospheres of cool stars do not take into account the effect of spots, plagues, and magnetic activity that could result in a significant amount of I-K excess (see also Stauffer et al. 2003). Interestingly, the effect of magnetic activity would explain not only the offset, but also the observed dispersion in the CM diagram. In this respect, we also mention the recent theoretical study by Chabrier et al. (2007), where an analysis of the effects of rotation and magnetic fields on the evolution of M dwarfs is presented. They show that rapid rotation and/or magnetic field in-

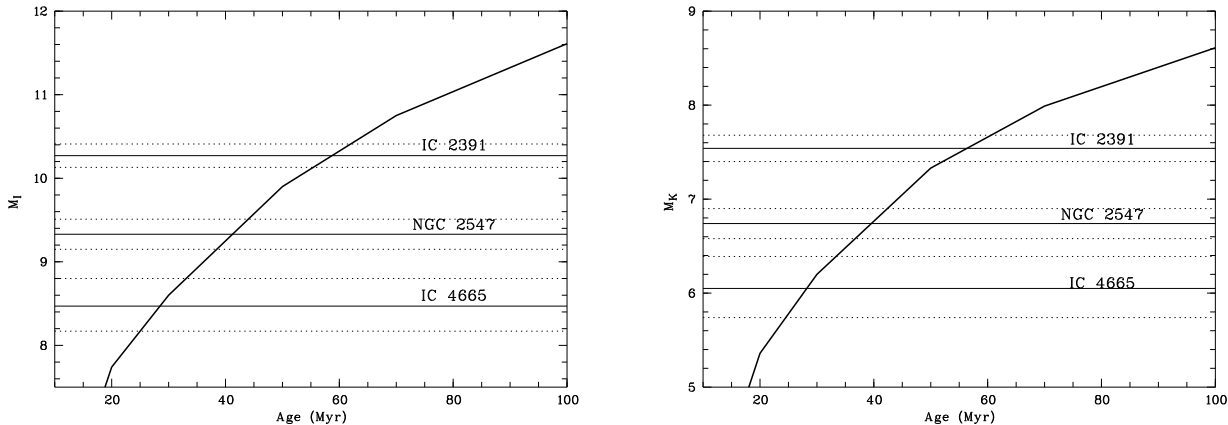


Figure 6. Location of currently known LDB of PMS clusters in absolute I_c (left) and K_s (right) magnitudes with uncertainties (dotted lines). Clusters are ordered from young to old: IC 4665, NGC 2547, IC 2391. The solid curve shows the predictions of the LDB as a function of age from the evolutionary models of Chabrier & Baraffe (1997) with $\alpha = 1$.

hibit convection, resulting in a reduced heat flow, and thus in larger radii and lower effective temperatures than for normal stars. As a consequence, the stars would appear younger in a color-magnitude diagram.

As to IC 2391, its sequence generally lies below those of IC 4665 and NGC 2547, yielding an age ~ 50 Myr in good agreement with the LDB age. Thus, we conclude that the overall distribution of cluster members shown in Fig. 7 indicates a smooth progression of increasing ages from IC 4665 to IC 2391.

5. Conclusions

We have obtained intermediate-resolution GIRAFFE spectra of 147 cluster candidate low-mass members of IC 4665. The spectra have been used to measure radial velocities and to establish the presence of the Li I 670.8 nm doublet and $H\alpha$ emission. Using these features as membership diagnostics, we have identified a subsample of 39 bona-fide cluster members with a mean radial velocity of $-15.95 \pm 1.13 \text{ km s}^{-1}$. From the distribution of these stars in the I_m vs. $I_m - z$ and K_s vs. $I_c - K_s$ color-magnitude diagrams, a clear separation of stars with and without Li is found. From this boundary, an age of $27.7^{+4.2}_{-3.5} \pm 1.1 \pm 2$ Myr is deduced, making IC 4665 the youngest known PMS cluster with an LDB determination. The model-dependent mass of the boundary corresponds to $M_* = 0.24 \pm 0.04 M_\odot$. Comparison of the LDB age with the standard TO age from Mermilliod (1981) and that inferred from isochrone fitting of the cluster low-mass sequence shows an excellent agreement, a result similar to that found in NGC 2547 by Jeffries & Oliveira (2005). This is at variance with the trend observed in older clusters (e.g., IC 2391, α Per, Pleiades) where the LDB age exceeds the TO nuclear age by a factor of ~ 1.5 .

The effort to find and characterize PMS clusters in the age range 5–50 Myr is being actively pursued by several groups and the first results are encouraging. In addition to the two similar clusters IC 4665 and NGC 2547 with age 25–35 Myr, two very young clusters have been found with ages ~ 10 Myr, namely NGC 7160 (Sicilia-Aguilar et al. 2005) and NGC 2169 (Jeffries

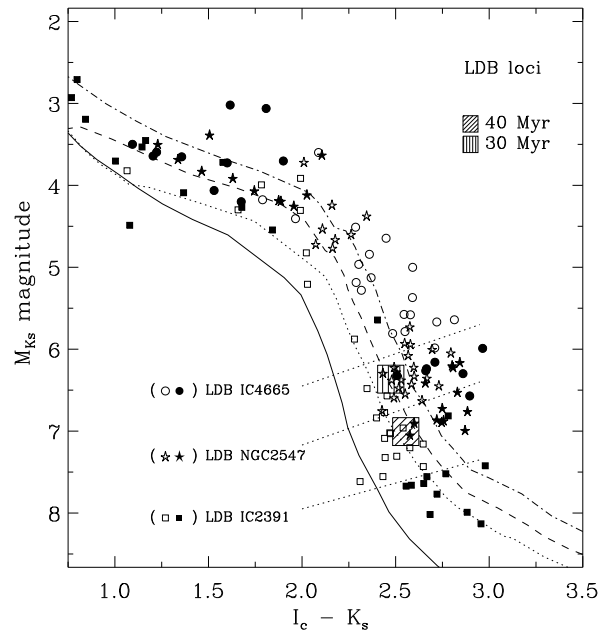


Figure 7. The distribution of confirmed members of IC 4665, NGC 2547, and IC 2391 in the K_s vs. $I_c - K_s$ diagram. Filled and empty symbols represent stars of each cluster with and without lithium, respectively. The hatched squares are the loci of the predicted LDB at different ages, according to the models of Baraffe et al. (2002). Also shown are the 20 (dot-dash), 30 (dash), and 50 Myr (dotted) isochrones from the same models, along with the ZAMS (solid line). The light diagonal curves mark the position of the LDB in each cluster, as labeled.

et al. 2007), as well as several young moving groups in the solar neighborhood (e.g., TW Hya, η Cha, Cha-Near; see Zuckerman & Song 2004). Now, the next observational challenge is to fill in the age gap with clusters between ~ 10 and 30 Myr to extend our knowledge on fundamental processes related to the early

evolution of stars and circumstellar disks, as well as on star forming process and its duration.

Acknowledgements. We thank the ESO Paranal staff for performing the service mode observations. We thank the referee, Dr. J. Stauffer, for the very useful suggestions. We are grateful to Germano Sacco for providing help with the maximum likelihood analysis of radial velocities. This work has made extensive use of the services of WEBDA, ADS, CDS etc. WJDW is grateful for the warm hospitality and support of the Osservatorio di Arcetri. The research of F. Palla and S. Randich has been supported by an INAF grant on *Young clusters as probes of star formation and early stellar evolution*.

References

- Baraffe, I., Chabrier, G., Allard, F., Hauschildt, P. H. 1998, *A&A*, 337, 403
- Baraffe, I., Chabrier, G., Allard, F., Hauschildt, P. H. 2002, *A&A*, 382, 563
- Barrado y Navascués, D., Stauffer, J. R., Jayawardhana, R. 2004, *ApJ*, 614, 386
- Basri, G., Marcy, G.W., Graham, J.R. 1996, *ApJ*, 458, 600
- Basri, G. 1997, *Mem. SAI*, 68, 917
- Bessell, M. S. 1979, *PASP*, 91, 589
- Bessell, M. S. 1991, *AJ*, 101, 662
- Bildsten, L., Brown, E. F., Matzner, C. D., Ushomirsky, G. 1997, *ApJ*, 482, 442
- Blecha, A., & Simond, G. 2004, Technical report, GIRAFFE BLDR Software - Reference Manual Version 1.12, Observatoire de Geneve
- Chabrier, G., Baraffe, I. 1997, *A&A*, 327, 1039
- Chabrier, G., Gallardo, J., Baraffe, I. 1997, *A&A*, 327, 1039
- Crampton, D., Hill, G., Fisher, W.A. 1976, *ApJ*, 204, 502
- Crawford, D.L., Barnes, J.V. 1972, *AJ*, 77, 862
- Dean, J. F., Warren, P. R., Cousins, A. W. J. 1978, *MNRAS*, 183, 569
- de Wit, W. J., Bouvier, J., Palla, F., et al. 2006, *A&A*, 448, 189
- Giampapa, M., Prosser, C.F., Fleming, T.A. 1998, *ApJ*, 501, 624
- Hogg, A.R., Kron, G.E. 1955, *AJ*, 60, 365
- Hoogerwerf, R., de Bruijne, J. H. J., de Zeeuw, P. T. 2001, *A&A*, 365, 49
- James, D. et al. 2008, Proceedings of the XIV Cambridge Workshop on Cool Stars, Stellar Systems, and the Sun, G. van Belle (ed), in press
- Jeffries, R. D. & Oliveira, J. M. 2005, *MNRAS*, 358, 13
- Jeffries, R. D., Oliveira, J. M., Naylor, T., Mayne, N.J., Littlefair, S.P. 2007, *MNRAS*, 376, 580
- Leggett, S.K., Allard, F., Berriman, G., Dahn, C.C., Hauschildt, P.H. 1996, *ApJS*, 104, 117
- Luyten, W. J. LB 1961, C24, 1L
- Martín, E.L., Montes, D. 1997, *A&A*, 318, 805
- Mermilliod, J. C. 1981, *A&A*, 97, 235M
- Mermilliod, J. C. 2000, *ASP Conf. Series*, 198, 105
- Pasquini, L., Avila, G., Blecha, A., et al. 2002, *Messenger*, 110, 1
- Prosser, C. F. 1993, *AJ*, 105, 1441P
- Prosser, C. F., Giampapa, M. S. 1994, *AJ*, 108, 964P
- Sicilia-Aguilar, Hartmann, L.W., Hernández, J., Briceño, C., Calvet, N. 2005, *AJ*, 130, 188
- Stauffer, J. R., Schultz, G., Kirkpatrick, J. D. 1998, *ApJ*, 499, L199
- Stauffer, J. R., Barrado y Navascués, D., Bouvier, J., et al. 1999, *ApJ*, 527, 219
- Stauffer, J.R. 2000, *ASP Conf. Ser.*, 198, p. 255
- Stauffer, J.R., Jones, B.F., Bouvier, J., et al. 2003, *AJ*, 126, 833
- Ushomirsky, G., Matzner, C.D., Brown, E.F., et al. 1998, *ApJ*, 497, 253
- Zuckerman, B., Song, I. 2004, *ARA&A*, 42, 685

Online Material

Table 1. The 147 candidate members of IC 4665 observed with FLAMES.

#	α_{2000}	δ_{2000}	Ref.	Name	I_m (mag)	z (mag)	V_{rad} (km/s)	δV_{rad} (km/s)	Li	H α	Mem.
1	17 44 45.015	+06 02 11.45	4	D.08.2.901	14.691	14.228	-41.0	0.8	N	abs	N
2	17 44 47.666	+06 01 52.78	1	P176	—	—	var	—	N	abs	N
3	17 44 48.120	+06 02 01.22	3	D.08.2.877	15.350	14.731	-29.0	3.0	N	em	N
4	17 44 48.354	+05 55 13.39	3	B.05.30.194	17.461	16.764	var	—	?	em	?
5	17 44 51.438	+05 49 53.39	1	P188	—	—	-15.0	3.0	N	abs	N
6	17 44 52.493	+05 48 35.43	1	P059	12.614	12.346	-14.7	1.0	Y	abs	Y
7	17 44 55.122	+05 49 40.43	1	P195	15.763	15.395	-47.0	3.0	N	abs	N
8	17 44 57.268	+05 47 20.14	3	A.00.30.2558	16.390	15.74	-24.0	4.0	N	abs	N
9	17 44 58.103	+05 51 32.93	1	P060	12.623	12.295	-15.0	1.0	Y	abs	Y
10	17 45 01.560	+05 56 22.32	1	P202	15.529	15.116	-66.7	1.4	N	abs	N
11	17 45 01.919	+05 51 55.58	1	P204	16.537	16.102	SB2	—	?	em	?
12	17 45 02.388	+06 07 32.45	4	D.09.2.1536	12.841	12.526	-57.1	2.1	Y	abs	N
13	17 45 03.655	+05 54 33.05	1	P206	13.674	13.319	13.4	1.0	N	abs	N
14	17 45 07.463	+05 50 59.39	1	P064	13.035	12.766	-53.6	0.6	N	abs	N
15	17 45 10.071	+05 49 21.50	1	P214	14.124	13.863	-55.3	0.4	N	abs	N
16	17 45 10.481	+05 46 17.38	1	P215	13.413	13.154	-14.6	1.0	Y	abs	Y
17	17 45 10.869	+05 47 57.40	1	P216	16.074	15.614	-61.7	3.0	N	abs	N
18	17 45 10.906	+05 56 06.81	1	P217	15.757	15.246	-66.0	2.0	N	abs	N
19	17 45 11.719	+05 45 25.30	1	P220	17.183	16.743	—	—	N	abs	N
20	17 45 12.935	+05 49 50.54	1	P065	12.440	12.17	var	—	Y	abs	Y?
21	17 45 13.301	+05 55 34.93	1	P222	13.651	13.312	-41.7	1.1	N	abs	N
22	17 45 14.971	+05 49 42.24	1	P067	13.912	13.66	57.2	1.5	N	abs	N
23	17 45 15.190	+06 07 44.77	3	D.09.30.3076	16.975	16.316	-47.0	4.0	Y	em	N
24	17 45 16.699	+05 53 56.41	1	P227	15.439	15.012	-11.0	2.0	N	abs	N
25	17 45 18.453	+05 44 58.84	1	GPF98-R05	17.265	16.639	-7.0	3.0	N	em	N
26	17 45 19.395	+05 47 40.13	1	P071	12.696	12.493	-15.3	1.3	Y	abs	Y
27	17 45 19.980	+05 46 29.53	1	P232	14.147	13.804	-15.1	1.2	N	em	Y
28	17 45 20.486	+05 53 20.74	1	P233	16.074	15.501	-15.8	2.0	N	em	Y
29	17 45 20.867	+05 54 27.68	4	A.00.2.270	12.761	12.483	-37.7	1.5	N	abs	N
30	17 45 22.039	+05 58 25.67	4	D.09.2.377	12.823	12.528	28.3	1.5	N	abs	N
31	17 45 23.174	+05 57 06.51	1	P238	16.928	16.314	-14.0	4.0	?	em	Y?
32	17 45 24.851	+06 00 07.91	3	D.09.30.1207	16.486	15.841	-69.0	4.0	N	abs	N
33	17 45 25.078	+05 51 38.75	1	P075	12.697	12.492	-15.8	1.5	Y	abs	Y
34	17 45 29.077	+05 45 09.24	3	A.01.30.3322	17.716	16.964	—	—	N	abs	N
35	17 45 30.051	+05 48 49.04	2	P242	15.139	14.719	25.6	1.0	N	abs	N
36	17 45 30.139	+05 47 07.46	3	A.01.2.1244	14.913	14.405	-15.0	2.0	N	abs	N
37	17 45 30.454	+05 58 22.28	4	D.10.2.409	12.883	12.595	22.0	1.8	N	abs	N
38	17 45 33.091	+05 46 24.35	1	P155	12.488	12.111	-46.0	1.0	N	abs	N
39	17 45 35.903	+05 49 04.33	1	P250	13.513	13.25	-68.0	1.5	N	abs	N
40	17 45 37.654	+05 53 53.40	1	P155	12.830	12.515	71.7	1.0	N	abs	N
41	17 45 37.837	+05 45 33.41	1	P251	15.201	14.861	var	—	N	abs	N
42	17 45 38.302	+05 44 44.30	1	P253	16.226	15.812	-11.0	2.0	N	abs	N
43	17 45 39.968	+05 45 16.25	1	P258	—	—	—	—	N	abs	N
44	17 45 41.023	+05 54 23.47	1	P260	15.378	15.005	-14.8	2.0	N	abs	N
44	17 45 42.415	+05 55 41.13	4	D.10.2.38	13.177	12.837	-2.8	1.5	N	abs	N
46	17 45 43.521	+05 55 56.46	1	P262	17.152	16.624	—	—	N	abs	N
47	17 45 44.987	+05 49 51.57	9	LB-3885	17.059	16.943	70.0	4.0	N	abs	N
48	17 45 56.008	+05 52 45.17	1	P272	16.570	16.069	SB2	—	N	abs	N
49	17 45 56.492	+05 48 44.64	1	K057	—	—	var	—	N	abs	N
50	17 45 56.733	+05 52 24.04	1	P273	14.505	14.135	6.1	1.0	N	abs	N
51	17 45 59.539	+05 50 45.52	1	P276	13.654	13.395	16.0	1.5	Y	abs	N
52	17 45 59.912	+05 36 18.05	1	P277	16.098	15.649	-25.0	2.0	N	abs	N
53	17 46 01.560	+05 37 11.58	1	P278	15.458	15.101	10.0	1.0	N	abs	N
54	17 46 01.604	+05 36 52.79	2	P279	15.155	14.695	20.0	1.0	N	abs	N
55	17 46 03.252	+05 33 12.58	1	P283	15.474	14.987	-19.6	3.0	N	em	Y?
56	17 46 03.384	+05 50 57.51	1	P284	16.435	15.935	-38.0	3.0	N	em	N
57	17 46 03.508	+05 49 42.63	2	P285	15.813	15.335	-47.0	4.0	N	abs	N
58	17 46 05.764	+05 41 54.62	2	P286	15.442	15.008	-110.0	4.0	N	abs	N
59	17 46 09.712	+05 40 58.13	1	P290	13.443	13.134	var/SB2	—	Y	abs/em	Y?

Table 1. continued.

#	α_{2000}	δ_{2000}	R	Name	I_m (mag)	z (mag)	V_{rad} (km/s)	δV_{rad} (km/s)	Li	H α	Mem.
60	17 46 10.312	+05 30 56.34	3	A.08.30.655	16.940	16.241	-16.0	4.0	Y	em	Y
61	17 46 10.811	+05 42 21.47	1	P292	—	—	20.0	10.0	N	abs	N
62	17 46 11.975	+05 41 25.85	1	P100	13.074	12.841	-16.9	0.6	Y	em	Y
63	17 46 12.634	+05 38 54.72	1	P296	13.940	13.642	-7.5	0.4	N	abs	N
64	17 46 13.813	+05 30 21.42	2	P298	16.203	15.681	-21.0	4.0	N	abs	N
65	17 46 14.048	+05 36 17.15	1	P300	16.916	16.365	-34.0	2.0	N	abs	N
66	17 46 15.183	+05 29 25.29	1	P101	12.761	12.359	-72.1	0.7	N	abs	N
67	17 46 15.234	+05 33 51.83	1	P303	15.542	15.110	-16.0	2.0	N	abs	N
68	17 46 17.791	+05 45 08.95	1	P306	13.344	13.068	28.8	0.5	N	abs	N
69	17 46 18.999	+05 46 20.37	1	P309	—	—	-16.0	1.0	N	em	Y
70	17 46 20.068	+05 45 00.19	1	P311	16.226	15.747	-170	10	N	abs	N
71	17 46 21.270	+05 29 14.80	2	P313	16.736	15.995	var	—	Y	em	Y?
72	17 46 23.313	+05 37 17.87	2	P315	14.876	14.398	var	—	N	em	Y?
73	17 46 23.892	+05 47 26.94	1	P317	14.151	13.804	6.4	0.7	N	abs	N
74	17 46 24.778	+05 35 38.13	1	P108	12.718	12.542	-16.0	3.0	Y	abs	Y
75	17 46 27.231	+05 29 28.57	2	P320	16.096	15.559	20.0	5.0	N	em	N
76	17 46 28.403	+05 40 18.02	1	P322	13.858	13.598	35.5	0.6	N	abs	N
77	17 46 28.923	+05 33 45.03	1	P323	15.650	15.290	-25.4	0.8	N	abs	N
78	17 46 29.136	+05 31 19.95	1	P113	13.421	13.174	-3.9	0.7	N	abs	N
79	17 46 29.480	+05 28 45.69	1	P326	13.672	13.303	-54.1	0.9	N	abs	N
80	17 46 30.256	+05 30 32.08	1	P328	14.353	14.044	-4.8	0.6	N	abs	N
81	17 46 30.476	+05 29 13.98	1	P329	15.589	15.162	SB2	—	N	abs	N
82	17 46 31.736	+05 28 35.03	3	A.09.30.47	15.940	15.291	-17.5	6.0	N	em	Y
83	17 46 33.977	+05 40 54.06	1	P331	13.705	13.449	-17.4	0.5	N	abs	Y
84	17 46 34.512	+05 48 53.10	1	P332	13.231	12.979	10.1	1.2	N	abs	N
85	17 46 34.731	+05 33 33.56	2	P333	16.706	16.069	-17.0	3.0	Y	em	Y
86	17 46 35.156	+05 26 28.85	1	P334	—	—	-43.0	2.0	N	abs	N
87	17 46 35.303	+05 36 10.62	2	P335	15.902	15.318	-12.0	6.0	N	em	Y?
88	17 46 35.530	+05 31 07.58	2	P336	14.910	14.443	-18.0	1.0	N	em	Y
89	17 46 37.712	+05 40 06.38	1	P337	16.568	16.105	5.0	1.0	N	abs	N
90	17 46 38.379	+05 35 48.63	2	P338	16.685	16.100	-17.0	4.0	Y	em	Y
91	17 46 40.649	+05 28 54.13	1	P339	13.822	13.455	52.6	0.6	N	abs	N
92	17 46 40.649	+05 40 19.82	1	P341	16.819	16.329	-43.0	2.0	N	abs	N
93	17 46 40.811	+05 28 21.36	3	A.09.30.14	16.840	16.118	-13.6	2.0	?	em	Y?
94	17 46 40.906	+05 49 02.67	1	P344	16.650	16.047	-16.0	2.0	Y?	em	Y
95	17 46 41.001	+05 44 18.42	1	P343	15.228	14.778	-15.0	4.0	N	em	Y
96	17 46 42.209	+05 33 41.98	1	P346	13.988	13.715	-82.8	0.4	N	abs	N
97	17 46 43.323	+05 35 14.01	1	P347	14.768	14.407	27.0	1.0	N	abs	N
98	17 46 43.770	+05 30 07.65	1	P348	15.741	15.177	-17.0	1.0	N	em	Y
99	17 46 45.146	+05 26 58.24	1	P349	13.306	13.043	119.8	0.7	Y	abs	N
100	17 46 45.359	+05 45 06.06	2	P350	16.475	15.854	-13.4	3.0	N	em	Y
101	17 46 46.337	+05 37 09.58	9	LB3900	17.270	17.018	-43.0	1.0	N	abs	N
102	17 46 46.575	+05 35 06.85	1	P352	13.325	13.108	43.2	0.5	N	abs	N
103	17 46 46.736	+05 49 09.35	1	P119	12.807	12.526	-42.9	0.7	N	abs	N
104	17 46 46.831	+05 47 05.15	1	P120	13.251	12.965	10.4	0.6	N	abs	N
105	17 46 47.622	+05 31 38.05	2	P354	15.278	14.800	-16.0	3.0	N	em	Y
106	17 46 48.113	+05 47 58.74	1	P121	—	—	84.0	2.6	N	abs	N
107	17 46 48.743	+05 43 00.62	1	P122	13.803	13.504	-4.8	2.3	N	abs	N
108	17 46 48.823	+05 41 59.01	2	P359	16.276	15.757	-38.0	4.0	N	abs	N
109	17 46 48.970	+05 48 54.98	1	P360	15.853	15.451	-35.0	1.0	N	abs	N
110	17 46 50.237	+05 36 41.06	1	P362	15.785	15.41	-56.0	3.0	N	em	N
111	17 46 51.848	+05 31 27.73	1	P364	16.027	15.614	-79.0	1.0	N	abs	N
112	17 46 52.200	+05 32 36.92	1	P123	14.059	13.780	49.9	0.4	N	abs	N
113	17 46 53.013	+05 32 47.02	1	P366	14.083	13.799	-83.3	0.6	N	abs	N
114	17 46 54.082	+05 31 26.18	1	P367	17.898	17.292	-65.0	4.0	N	abs	N
115	17 46 54.719	+05 41 59.74	3	A.10.30.3980	17.854	17.108	var	—	?	em	?
116	17 46 54.990	+05 37 45.17	1	P126	13.465	13.149	101	0.8	N	abs	N
117	17 46 55.159	+05 41 12.70	2	P369	16.322	15.715	-37.0	3.0	N	em	N
118	17 46 55.620	+05 30 29.42	2	P370	15.412	14.962	6.0	4.0	N	abs	N

Table 1. continued.

#	α_{2000}	δ_{2000}	R	Name	I_m (mag)	z (mag)	V_{rad} (km/s)	δV_{rad} (km/s)	Li	H α	Mem.
119	17 46 56.016	+05 38 34.99	2	P372	16.608	16.028	-18.0	4.0	Y?	em	Y
120	17 46 56.418	+05 47 44.62	1	P374	14.554	14.155	-16.2	0.8	N	em	Y
121	17 46 56.638	+05 36 07.30	2	P373	16.169	15.537	-16.0	2.0	N	em	Y
122	17 46 58.696	+05 47 26.03	1	P375	13.377	13.111	-3.5	0.8	N	abs	N
123	17 46 59.033	+05 45 44.77	3	A.04.2.1503	14.966	14.422	-51.0	3.0	N	abs	N
124	17 46 59.319	+05 30 10.30	1	P129	12.509	12.149	-116.9	0.6	N	abs	N
125	17 47 00.227	+05 30 29.04	1	P377	13.680	13.403	-17.0	2.0	Y	abs	Y
126	17 47 01.787	+05 45 22.94	1	P379	16.281	15.799	-13.0	2.0	N	abs	N
127	17 47 01.912	+05 30 45.41	2	P378	17.119	16.568	—	—	N	abs	N
128	17 47 03.098	+05 34 46.35	2	P380	16.116	15.544	-17.1	2.0	N	em	Y
129	17 47 05.288	+05 43 31.34	1	P132	12.882	12.612	-15.1	0.6	N	abs	N
130	17 47 06.467	+05 28 04.14	1	P382	13.829	13.587	-2.6	0.5	N	abs	N
131	17 47 07.595	+05 36 14.70	1	P383	14.467	14.221	25.0	1.0	N	abs	N
132	17 47 08.518	+05 37 37.65	4	A.10.2.1392	13.025	12.744	-113.3	0.8	N	abs	N
133	17 47 09.902	+05 28 13.37	1	P385	17.043	16.116	—	—	N	abs	N
134	17 47 09.961	+05 43 14.06	2	P387	15.674	15.239	-34.0	1.0	N	abs	N
135	17 47 09.968	+05 29 06.42	1	P386	14.712	14.175	-30.8	0.7	N	abs	N
136	17 47 11.030	+05 39 55.98	1	P390	13.596	13.324	61.1	0.6	N	abs	N
137	17 47 11.660	+05 33 09.98	3	A.10.30.1418	17.250	16.598	var	—	?	em	?
138	17 47 11.865	+05 29 24.78	3	A.10.30.316	16.236	15.566	-21.0	3.0	N	em	Y?
139	17 47 12.028	+05 43 00.54	9	IRAS17447+054	—	—	SB2?	—	N	abs	N
140	17 47 12.480	+05 36 33.85	1	P137	13.058	12.713	67.8	0.9	N	abs	N
141	17 47 12.532	+05 42 14.95	1	P394	—	—	-16.0	2.0	N	abs	N
142	17 47 16.282	+05 29 49.50	1	P396	13.844	13.457	-16.9	0.4	N	abs	Y
143	17 47 17.197	+05 31 24.08	4	A.11.2.358	12.509	12.204	33.7	0.5	N	abs	N
144	17 47 19.490	+05 44 47.38	3	A.05.30.3622	17.248	16.547	-16.0	3.0	Y	em	Y
145	17 47 19.497	+05 30 41.39	2	P398	15.373	14.789	-17.7	3.0	N	em	Y
146	17 47 19.636	+05 43 40.74	1	P399	16.290	15.745	-34.0	3.0	N	em	N
147	17 47 20.010	+05 46 53.71	2	P400	15.269	14.815	-16.2	2.4	N	em	Y